First results from MAST

A. Sykes, R.J. Akers, L.C. Appel, E.R. Arends[a], P.G. Carolan, N.J. Conway, G.F. Counsell, G. Cunningham, A. Dnestrovskij[b], Yu.N. Dnestrovskij[b], A.R. Field, S.J. Fielding, M.P. Gryaznevich, S. Korsholm[c], E. Laird[d], R. Martin, M.P.S. Nightingale, C.M. Roach, M.R. Tournianski, M.J. Walsh[e], C.D. Warrick, H.R. Wilson, S. You, MAST Team, NBI Team

Euratom–UKAEA Fusion Association,
Abingdon, Oxfordshire, United Kingdom

[a] FOM Insituut voor Plasmafysica Rijnhuizen, Nieuwegein, Netherlands
[b] Kurchatov Institute, Institute of Nuclear Fusion, Moscow, Russian Federation
[c] Risø National Laboratory, Roskilde, Denmark
[d] St. John's College, Oxford University, Oxford, United Kingdom
[e] Walsh Scientific Ltd, Abingdon, Oxfordshire, United Kingdom

Abstract. MAST is one of the new generation of large, purpose-built spherical tokamaks (STs) now becoming operational, designed to investigate the properties of the ST in large, collisionless plasmas. The first six months of MAST operations have been remarkably successful. Operationally, both merging–compression and the more usual solenoid induction schemes have been demonstrated, the former providing over 400 kA of plasma current with no demand on solenoid flux. Good vacuum conditions and operational conditions, particularly after boronization in trimethylated boron, have provided plasma current of over 1 MA with central plasma temperatures (ohmic) of order 1 keV. The Hugill and Greenwald limits can be exceeded and H mode achieved at modest additional NBI power. Moreover, particle and energy confinement show an immediate increase at the L–H transition, unlike the case of START, where this became apparent only at the highest plasma currents. Halo currents are small, with low toroidal peaking factors, in accordance with theoretical predictions, and there is evidence of a resilience to the major disruption.

1. Introduction

The MAST device now operational at Culham is essentially a scaled-up version of the successful START experiment [1] but with better vacuum conditions, with feedback controlled power supplies and with a plasma cross-section comparable to those of ASDEX-U and DIII-D. Key parameters of MAST and START are compared in Table 1.

MAST achieved first plasma in December 1998. Since that time the central solenoid has been rewound with improved insulation, a fully instrumented centre column has been fitted and two beamlines on loan from Oak Ridge National Laboratory (ORNL) have been installed and operation at up to 1 MW has been demonstrated. Extensive internal diagnostics have been installed to provide accurate magnetic reconstruction (with EFIT), to measure halo currents and divertor target parameters, etc.

2. Plasma induction

The plasma physics programme commenced in December 1999 with tests of the novel merging–compression technique whereby spherical tokamak (ST) plasmas can be produced without the need of any flux from the central solenoid. This technique, pioneered on START, utilizes a special feature of the START and MAST designs, namely that the poloidal field coils are inside the vacuum vessel, as shown in Fig. 1. The process involves the use of flux from the large radius P3 coils, rather than the central solenoid (P1), to initiate the plasma. The toroidal field is applied and initial deuterium gas injected into the tank. A large current is passed through the P3 coils and rapidly ramped down.

Breakdown occurs in the form of plasma rings around each P3 coil. The plasma rings attract and merge on the midplane as the P3 current reduces towards zero. Application of a vertical field from the P4 and P5 coils then compresses the plasma into

Table 1. Comparison of key parameters for MAST and START

	MAST		START (achieved)
	Design	Achieved	
Minor, major radius, a, R (m)	0.65, 0.85	0.65, 0.85	0.25, 0.32
κ (elongation)	$\leq$3	2.2	$\leq$3
Aspect ratio (R/a)	$\geq$1.3	1.3	$\geq$1.2
Plasma and toroidal field rod current (MA)	2, 2.2	1.05, 2.1	0.31, 0.5
Toroidal field at R (T)	0.52	0.51	0.31
Auxiliary heating			
P_{NBI} (MW)	5	1	1
P_{ECRH} (MW)	1.5	0.6	0.2
Pulse length (s)	1–5	0.5	$\leq$0.06
Bake-out temperature (°C)	200	140	50
Plasma volume (m^3)	10	10	0.5

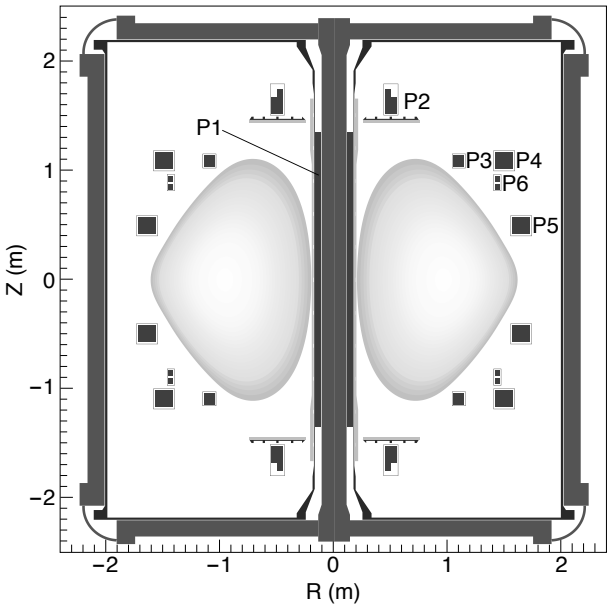

Figure 1. Plan view of MAST showing the PF coils.

the required ST configuration. ST plasmas at currents of up to 450 kA are routinely obtained by this merging–compression technique. The process is shown in Fig. 2.

The merging–compression scheme (discharge 2967) is compared with the more conventional direct induction scheme (2898) in Fig. 3. (It is important to note that, in this first campaign, the solenoid waveform is preset and not feedback controlled.) In direct induction, breakdown occurs in a poloidal field null, and sufficient electric field is provided by ramp-down of the solenoid current. The oscillations in loop voltage at the time of breakdown, present in both cases but larger in 2967, result from transient currents induced in the poloidal field coil cases. The stills shown in Fig. 2 may be referred to the waveform for 2967 shown in Fig. 3.

The merging–compression scheme is normally employed on MAST. After the ST plasma has been established, the central solenoid is then used to maintain or further increase the initial plasma current; plasma ramp rates of up to 13 MA/s at a loop voltage of 7 V can be achieved.

Double null divertor (DND) plasmas of up to 1 MA have been obtained using less than one half of the designed maximum flux swing of approximately 1 V s. Discharge 2482 (May 2000) obtained over 1 MA (Fig. 4) using ∼0.4 V s. The plasma had elongation ≈ 2 and an overall diameter of approximately 2.6 m. Heated by an NBI power of ∼650 kW, the plasma attained central electron and ion temperatures of over 1 keV.

3. Plasma conditioning

Vacuum conditions on MAST have been further improved by boronization, whereby a thin layer of boron is deposited over material surfaces by glow cleaning in a mixture of deuterated trimethylated boron and helium. A tenfold reduction in impurity emission was achieved (Fig. 5), and the plasma current obtained increased by 20% for the same loop voltage waveform.

Following the first boronization, the first H modes were observed in ohmic plasmas. These were limited on the centre column graphite, and occurred during the current decay phase when the aspect ratio was

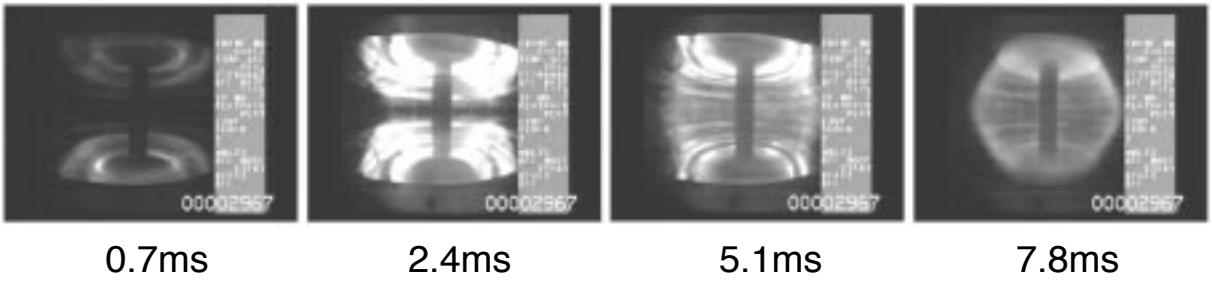

Figure 2. Stills from a high speed video showing plasma formation by merging–compression in MAST discharge 2967; times shown indicate elapsed time after ramp-down begins.

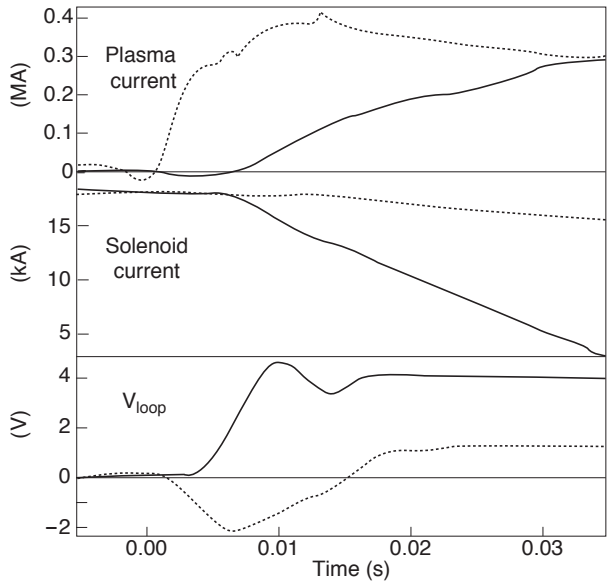

Figure 3. Direct induction and merging–compression schemes compared. In direct discharge 2898 (full lines), the solenoid current is ramped down to give an initial loop voltage of 4 V, which produces a plasma current ramp of ∼9 MA/s. In merging–compression discharge 2967 (dotted lines), the process produces 400 kA of plasma current before the solenoid ramp begins; the low ramp rate giving $V_{loop} \approx 1$ V is sufficient to maintain the plasma current.

relatively large (Fig. 6), demonstrating that conventional aspect ratio plasmas can also be studied in MAST.

4. Neutral beam injection

MAST is equipped with two NBI lines on loan from ORNL. At full specification, they are together designed to deliver 5 MW of 70 keV deuterium. During the first campaign, the south injector alone was operational and capable of delivering up to 800 kW of 30 keV hydrogen.

Although this power and energy were very similar to those employed on START, beam heating and current drive are predicted to be more effective on MAST owing to the higher fields and temperatures and larger plasma size: typical results of beam modelling using the LOCUST Monte Carlo code are shown in Fig. 7. It is seen that the orbit in START is less well confined and leaves the last closed flux surface (LCFS) of the plasma.

An $E\|B$ neutral particle analyser (NPA), on loan from Princeton Plasma Physics Laboratory (PPPL), has been installed at a tangency radius of 0.7 m to diagnose the fast ion population resulting from NBI and to measure changes in the bulk thermal plasma temperature. The NPA can measure H and D particle energies from 0.5 to 600 keV/amu for both H and D.

4.1. NBI heating on MAST

Heating of both electrons and ions is observed [2]. For example, the pair of discharges 2701 and 2704 are nominally identical except that 2701 had NBI heating of ∼530 kW at 30 keV, whereas 2704 was ohmic. The electron temperature profiles and the development of the central ion temperature are shown in Fig. 8.

In the NBI heated discharge 2701, the auxiliary heating was applied from 0.05 to 0.25 s, and at the end of this time the plasma thermal energy was double that in the ohmic discharge 2704. This increase in pressure produced the increase in plasma size seen in the T_e profile (the outer edge of the plasma extending beyond the range of the Thomson scattering diagnostic). Still further increases in stored energy are obtained if an L–H transition occurs, as discussed in the next section.

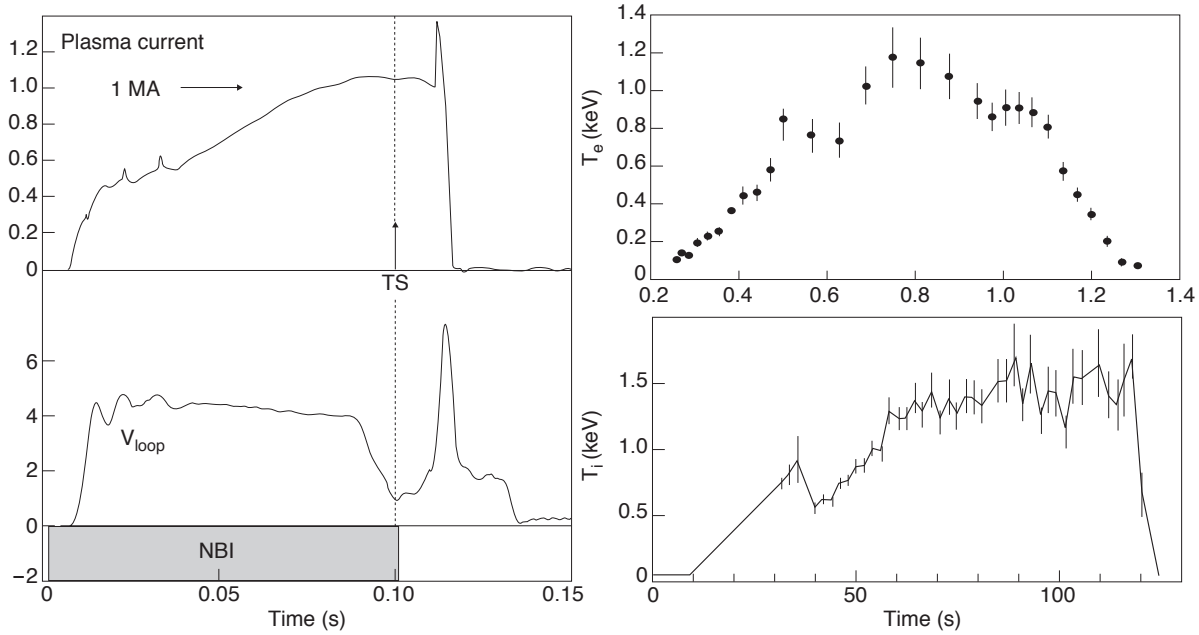

Figure 4. First 1 MA plasma on MAST, May 2000. As in all discharges during this first campaign, the solenoid waveform is preset and not feedback controlled. The Thomson scattering profile shows a central electron temperature of ∼1 keV, and the neutral particle analyser signal indicates a central ion temperature of ∼1 keV.

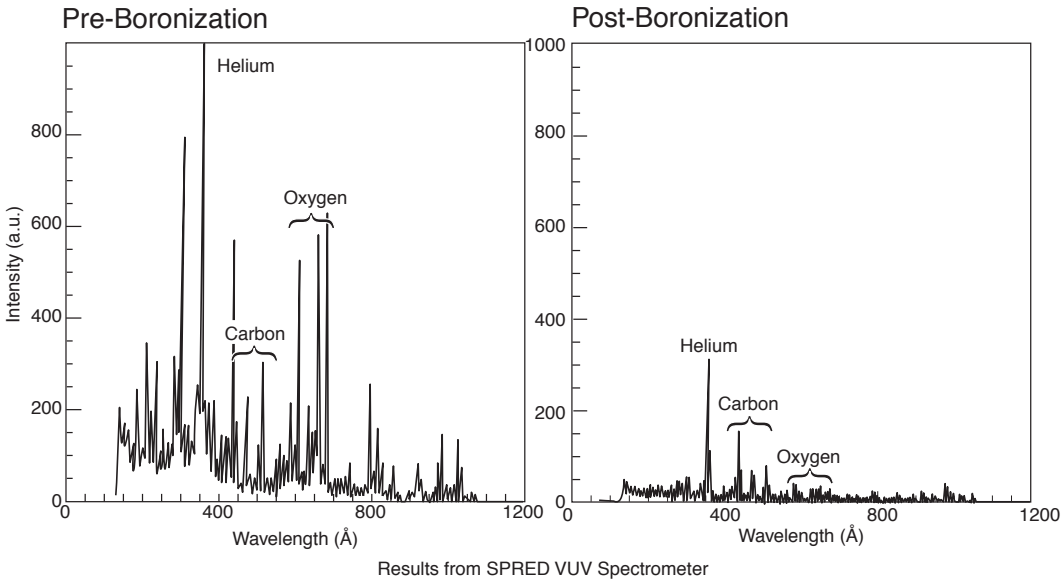

Figure 5. Plasma impurity fractions immediately before and after the first boronization of MAST.

4.2. H mode operation

First H modes at low aspect ratio were achieved in NBI heated plasmas in June 2000 [3]. The transition to H mode in MAST is clearly demonstrated in the pair of consecutive discharges 2700 and 2701 shown in Fig. 9. These had nominally identical parameters and appeared to be identical discharges until $t = 220$ ms — so much so that the sawtooth crashes almost coincide. However, 2700 achieved L–H

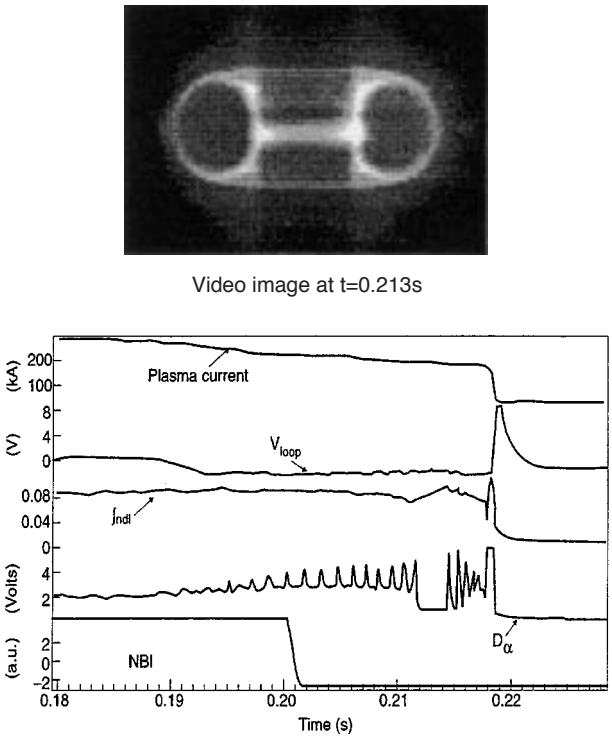

Figure 6. Observation of H mode during current ramp-down in ohmic MAST discharge 2821. The plasma aspect ratio at this time is $A = 2.1$ ($a \approx 0.18$ m, $R \approx 0.38$ m).

transition while 2701 did not. These discharges were part of a sequence of repeated discharges: the next discharge to achieve L–H transition was 2705. For these low power (∼530 kW) NBI heated discharges, transition appears to be a random occurrence; if it does occur, it always follows a sawtooth crash.

Although the transition is achieved at relatively low NBI power, the total (ohmic + NBI) power is typically 1.2 MW, which is a factor of ∼30 greater than the threshold power for L–H transition predicted by the usual scalings [4]. This was also the case in START [5] but may indicate non-optimal operational conditions rather than an inadequacy in the scaling law. Although some periods of regular ELMing have been observed in MAST discharges, most H mode discharges feature ELM free periods (of up to 60 ms) separated by giant ELMs, each ELM reducing the stored energy by up to 10%, as shown in Fig. 10.

5. Energy confinement

For START, both L mode and H mode confinement data are well represented by the ITER98pby1 scaling [1]. H mode discharges only exhibited a clear

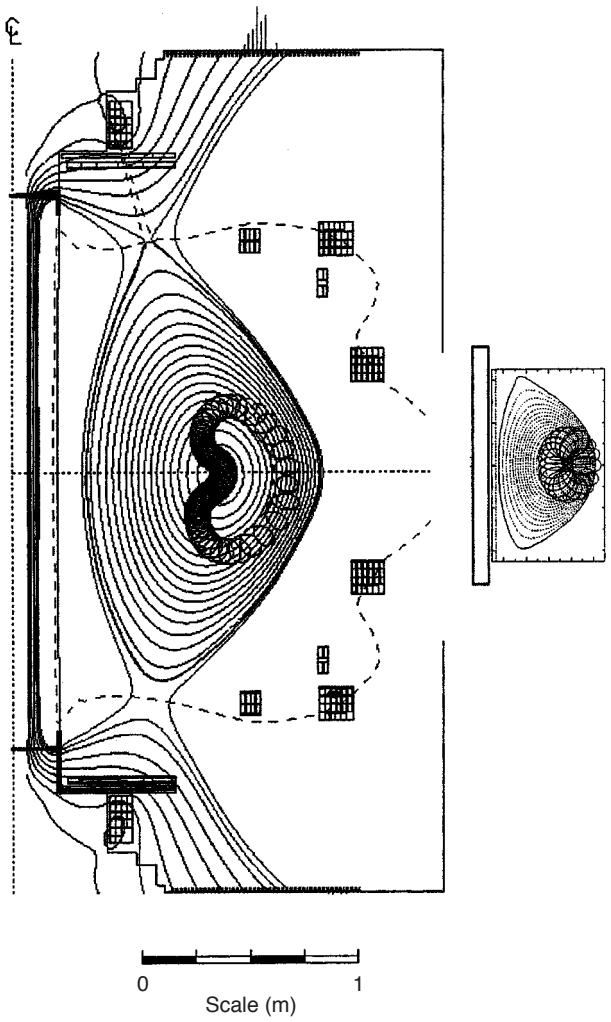

Figure 7. Comparison of 30 keV H orbits modelled using the LOCUST Monte Carlo code, in typical plasmas in MAST (left) and START (right, same scale).

improvement in confinement (compared with similar L mode discharges) at the highest plasma currents (>250 kA) achievable on START [5]. ELMy H mode confinement data have been submitted to the international database and are compared with confinement in world tokamaks in Fig. 11. By using a combination of magnetic reconstruction provided by EFIT and kinetic evaluations using Thomson scattering and NPA diagnostics, confinement has been estimated in a range of MAST discharges. Of particular interest is the change in confinement at the L–H transition. In the steady L mode period before transition to H mode in discharge 2700 the energy confinement is estimated to be ∼14 ms, compared with a prediction of 19 ms given by the ITER98pby1 scaling. After the L–H transition a rapid increase

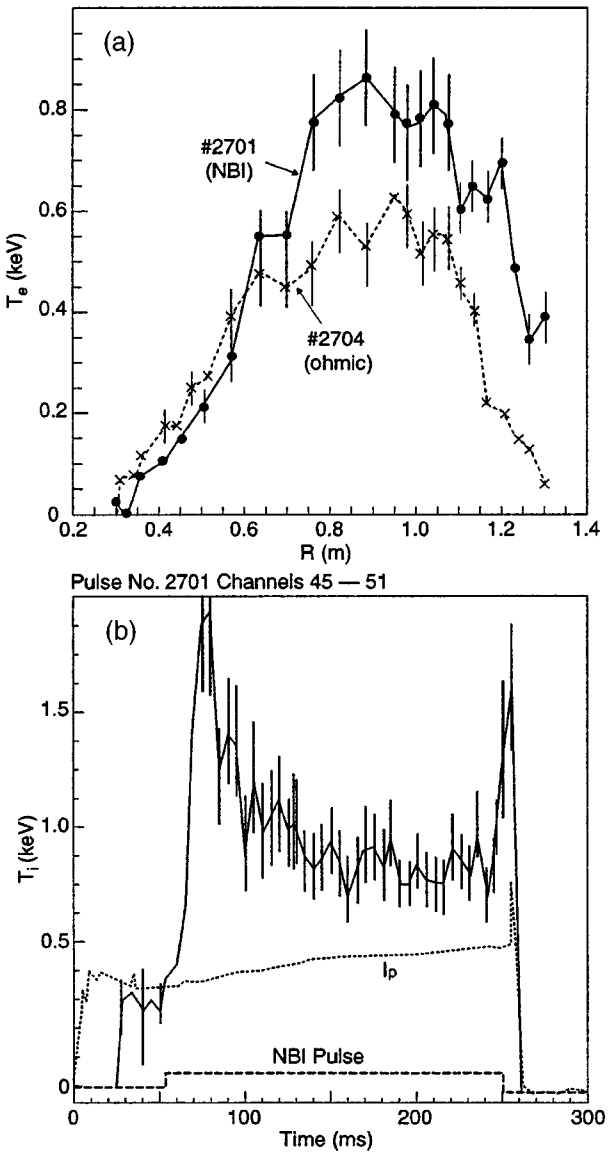

Figure 8. (a) NBI heating of electrons (measured by 30 point Thomson scattering) is shown by comparing NBI discharge 2701 with the companion ohmic discharge 2704. (B) In 2701 the central ion temperature (estimated from the NPA) increases from 300 to 700 eV after NBI.

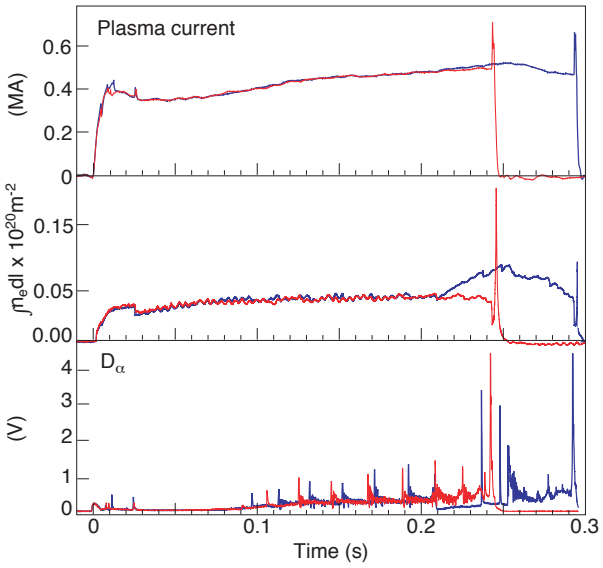

Figure 9. Waveforms of discharges 2700 (blue; L–H transition at 0.22 s) and 2701 (red; identical experimental parameters but no transition). Both discharges end in a vertical displacement event.

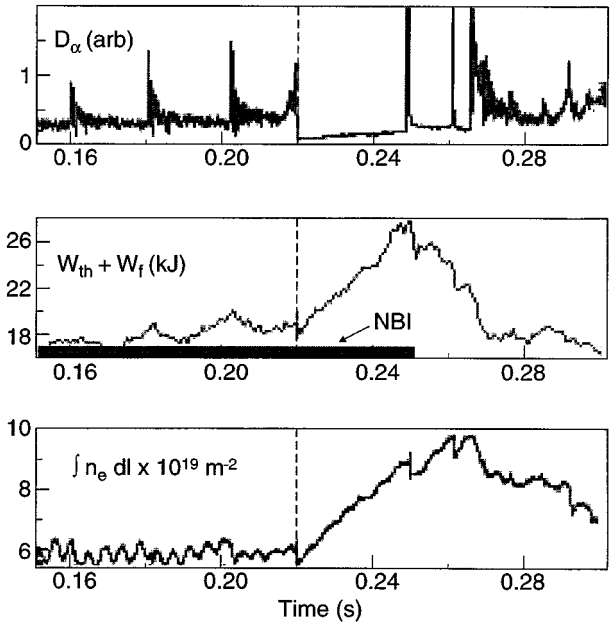

Figure 10. Details of L–H transition for MAST discharge 2700, showing midplane D_α emission, plasma stored energy (including the fast ion component) and line integral density.

in plasma thermal energy takes place, as shown in Fig. 10.

Accurate evaluation of confinement after the transition is difficult owing to the profile and plasma size changes accompanying the transition. Averaging over the period 218–250 ms (at which point the NBI is shut off), and subtracting an estimate of the fast ion contribution, a conservative estimate (evaluated at the centre of the period) is that confinement has doubled to 28 ms. The ITER98pby1 prediction has itself increased to 25 ms, giving an H factor of 1.1. This period includes a giant ELM. Although preliminary, these results indicate substantial improvements in confinement in H mode even at these low plasma

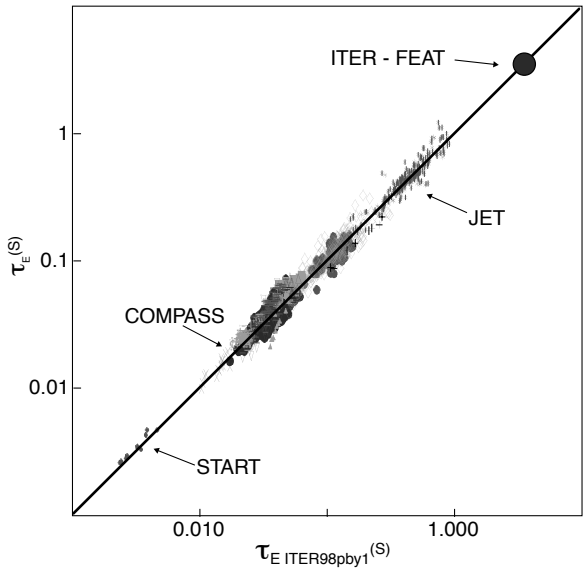

Figure 11. World tokamak ELMy H mode confinement data compared with the ITER98pby1 scaling.

currents. Modelling suggests [6] that this difference from START is due to the very high neutral density present in START. This causes increased charge exchange losses at the transition, whereas in MAST the neutral density is typically 50 times lower, owing mainly to the increased particle confinement time in the larger device.

6. Density limits

MAST discharges can exceed the Hugill and Greenwald limits, especially at low currents. These limits are here defined as $n_H = I_p$ (MA)$/(\pi a^2 \kappa)$ and $n_G = I_p/(\pi a^2)$, respectively, where n_H and n_G are line averaged densities in units of 10^{20} m^{-3}. By taking $\kappa = 1.8$ (typical of MAST DND discharges) they can be compared on a single plot (Fig. 12).

It is seen that although the highest density shots have NBI heating, there is not a marked difference between ohmic and NBI heated discharges (at least for these relatively low power NBI discharges), and several ohmic shots exceed the Greenwald limit.

The trace in Fig. 12 shows the time evolution of discharge 2910, which had a relatively high NBI power of ∼770 kW and attained Greenwald number $G \approx 1.4$ ($G = n/n_G$). This shot had a MARFE at the time circled (evidenced on visual diagnostics as a toroidally symmetric ring of light on the centre column, which moved past the midplane, giving a 'blip' on the midplane interferometer). Other discharges

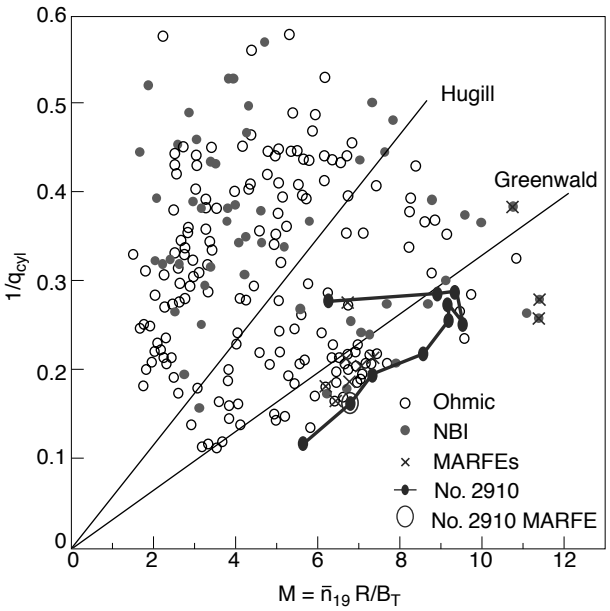

Figure 12. Operation space for MAST ohmic and NBI discharges (summer 2000), assuming $q_{cyl} = 2.5a^2 \times(1+\kappa^2)B_T/RI_p$ and $\kappa = 1.8$.

exhibiting MARFEs, which on MAST have so far occurred close to the Greenwald limit, are shown as crosses in Fig. 12; the MARFEs are transient and do not cause radiation collapse or disruption.

7. Halo currents in MAST

Spherical tokamaks have good vertical stability at high 'natural' elongation ($\kappa \approx 1.8$, dependent upon current profile), where 'natural' means the elongation present in a uniform vertical field. A destabilizing vertical field produces higher elongations which can lead to vertical displacement events (VDEs). Indeed many MAST discharges in this first campaign ended in a VDE as the stray field from the (uncompensated) solenoid became increasingly destabilizing as the discharge proceeded. Although theory and modelling predict that forces due to halo currents should be relatively low in the ST [7, 8], it is important to verify this as MAST is designed for operation at up to 2 MA, and a comprehensive set of halo current diagnostics have been installed and commissioned [9].

Results to date are shown in Fig. 13. It is seen that the currents (and forces) induced at a VDE are much lower than those met in tokamaks of conventional aspect ratio.

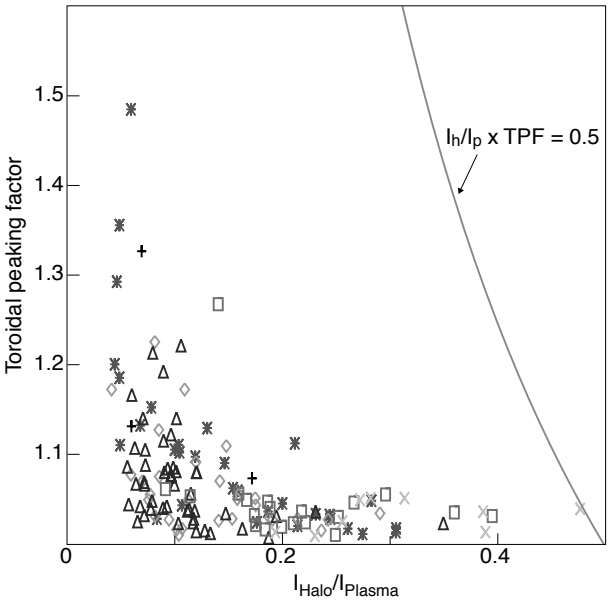

Figure 13. Halo current fraction and toroidal peaking factor (TPF), calculated at the time of maximum halo current. The line indicates a typical design constraint for ITER-FEAT [10]; the points having the highest halo fractions are low current, higher aspect ratio discharges.

8. Current terminations

Inspection of I_p waveforms and high speed video recordings shows that many MAST discharges appear to end abruptly. Most of these events are actually VDEs, usually triggered by an internal reconnection event (IRE). At the end of the solenoid swing, the solenoid current is brought back to zero, producing a negative loop voltage, which causes changes in the plasma current profile and often an IRE. The combination of IRE, destabilizing vertical field and unoptimized vertical feedback system often leads to a VDE. In the next campaign it is intended to reduce the solenoid stray field by use of the P2 compensation coils and, with improvements in the vertical feedback system, most VDEs should be avoidable.

It is important to know how susceptible STs are to other sorts of rapid termination. On START it was found that the plasma had a high degree of resilience to major disruptions [11]. In MAST, disruptions have not been observed during the current ramp-up phase or when exploring the density limit (unless q_{95} is very low). Figure 14 shows a comparison of VDE and major disruption terminations on MAST. As can be seen, in a VDE the plasma moves

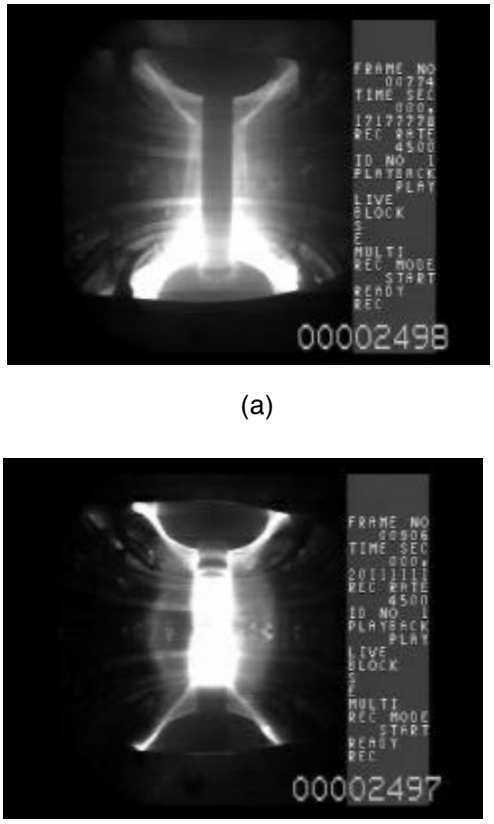

Figure 14. High speed video stills of (a) a VDE and (b) a disruption.

abruptly up or down, whereas in a major disruption it remains in the midplane region.

High current MAST discharges do not disrupt directly. They suffer a series of IREs which reduce the current gradually, as shown in Fig. 15, so that there is a range of possible points at which the plasma current (and other parameters) can be taken. The convention adopted, as shown in Fig. 15, is that parameters are measured at the last current dip before I_p goes to zero.

From the most recent 1198 shots, 60 non-VDE disruptions were found, with I_p between 40 and 265 kA. The final disruption is at lower current and, because the vertical field is not usually reduced accordingly, occurs where R is small and A is high (Fig. 16). Of the disruptions at aspect ratios of <1.8, it is seen that all except two occur during the final ramp-down of plasma current. Of these two, the higher current discharge is 2828, shown in Fig. 15.

These results suggest that MAST has indeed considerable resilience to the major disruption;

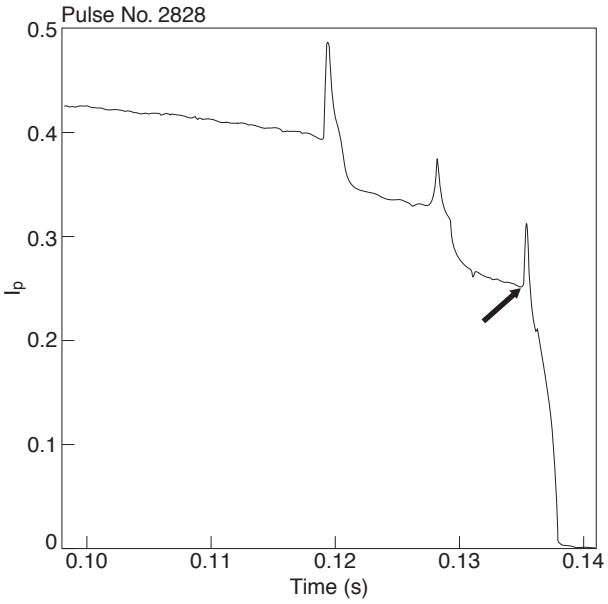

Figure 15. Convention used for definition of disruption parameters.

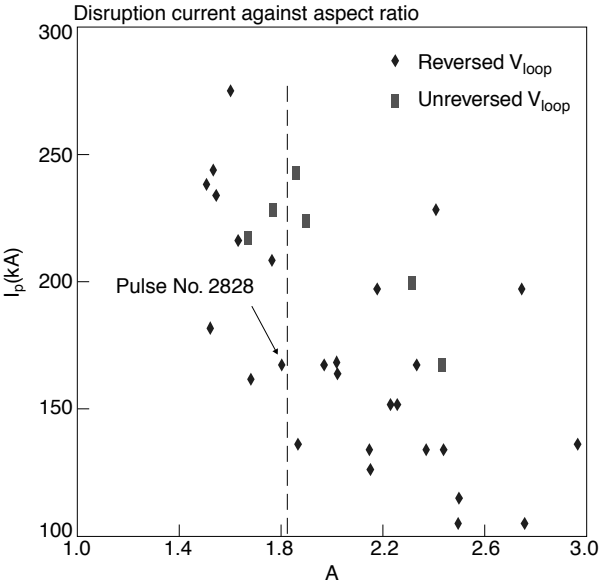

Figure 16. Plot of plasma current at disruption against aspect ratio. Disruptions for which V_{loop} is positive or zero are shown as squares, others as diamonds. The dashed line at $A = 1.8$ divides disruptions in the ST regime from those in the non-ST regime.

moreover, it is considered that this could be further improved by field control during the current ramp-down phase. It is noteworthy that in this first MAST campaign, a high current termination

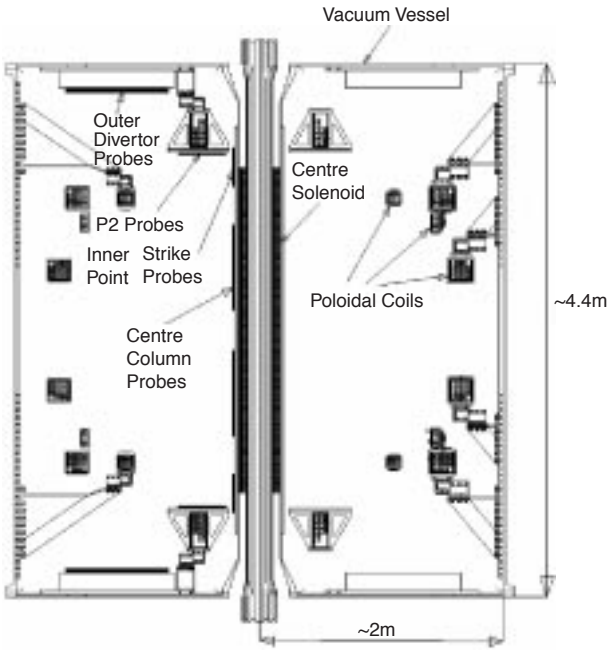

Figure 17. Location of Langmuir probes (576 in all) in MAST.

occurred only if an IRE led to a vertical instability, as occurred for discharges 2700 and 2701, shown in Fig. 9. This may be avoidable by vertical field control and/or improved vertical feedback systems.

9. Divertor power loading studies in MAST

The SOL plasma parameters and power loadings in DND ST geometry were measured and analysed for the first time on START [12], where several unusual features were observed, including strong in–out/up–down power asymmetries and significant SOL currents. However, analysis of the data was complicated by a blanket of high neutral density surrounding the START plasma (a result of the fuelling scheme, fully open divertor geometry and large vessel to plasma volume ratio), which was believed to give rise to large charge exchange losses from the SOL.

MAST is well equipped with arrays of high spatial resolution, swept Langmuir probe arrays (576 probes in total) covering all four strike point regions [13] (Fig. 17). For ohmic plasmas, densities and temperatures in both the outboard and inboard SOLs produce strongly collisional conditions ($\nu^* > 7$ and 50, respectively) with midplane heat flux density

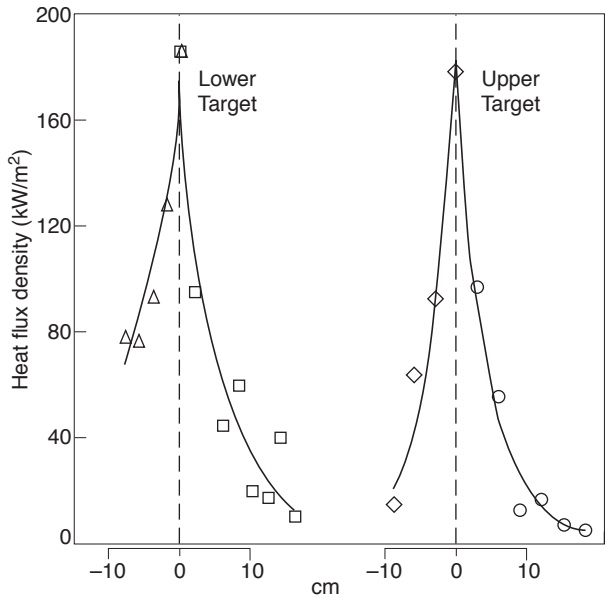

Figure 18. Heat flux density profiles across the lower and upper outboard strike points at time 144 ms for discharge 2321. To the right of the separatrix (dotted line) is the SOL, to the left the private flux region.

scale lengths of order 6 mm at both positions. All the plasma parameter scale lengths are significantly broadened on the outboard side as a result of strong poloidal flux expansion ($f_{exp} > 7$) (Fig. 18).

About two thirds of the power entering the SOL reached the targets, compared with one third on START (the difference probably arising from higher charge exchange losses in START). The ratio of the average power to the outboard targets to the average power to the inboard targets was ∼6.5:1. Since this exceeds the ratio of ∼3:1 for the outboard and inboard separatrix surface areas, the power loading on the inboard strike point may not be as critical for the ST as was initially supposed.

10. Conclusions

The first six months of MAST operations have been remarkably successful. Operationally, both merging–compression and the more usual solenoid induction schemes have been demonstrated, the former providing over 400 kA of plasma current with no demand on solenoid flux. Good vacuum and operational conditions, particularly after boronization with trimethylated boron, have enabled the attainment of a plasma current of over 1 MA with central plasma temperatures (ohmic) of order 1 keV. The Hugill and Greenwald limits can be significantly exceeded and H mode achieved at modest additional NBI power. Moreover, particle and energy confinement show an immediate increase at the L–H transition, unlike the case of START, where this became apparent only at the highest plasma currents. Halo currents are small, with low toroidal peaking factors, in accordance with theoretical predictions, and there is evidence of a resilience to the major disruption.

These results, together with those from the other new STs now commencing operation, will rapidly increase understanding of the physics properties of the ST and determine its potential for a future fusion device.

Acknowledgements

This work is funded jointly by the United Kingdom Department of Trade and Industry and Euratom. The NBI equipment is on loan from ORNL, the NPA is on loan from PPPL and EFIT is supplied by General Atomics.

References

[1] Sykes, A., et al., Nucl. Fusion **39** (1999) 1271.
[2] Akers, R., et al., in Fusion Energy 2000 (Proc. 18th Int. Conf. Sorrento, 2000), IAEA, Vienna (2001) CD-ROM file EXP4/19 and http://www.iaea.org/programmes/ripc/physics/fec2000/html/node1.htm.
[3] Gryaznevich, M., in Controlled Fusion and Plasma Physics (Proc. 27th Eur. Conf. Budapest, 2000), Vol. 24B, European Physical Society, Geneva (2001) CD-ROM file D1-004.
[4] Snipes, J.A., in Controlled Fusion and Plasma Physics (Proc. 24th Eur. Conf. Berchtesgaden, 1997), Vol. 21A, Part III, European Physical Society, Geneva (1997) 961.
[5] Sykes, A., et al., Phys. Rev. Lett. **84** (2000) 495.
[6] Dnestrovskij, Yu.N., et al., Plasma Phys. Rep. **26** (2000) 539.
[7] Caloutsis, A., Gimblett, C.G., Nucl. Fusion **38** (1998) 1487.
[8] Pomphrey, N., Bialek, J.M., Park, W., Nucl. Fusion **38** (1998) 449.
[9] Martin, R., et al., in Controlled Fusion and Plasma Physics (Proc. 27th Eur. Conf. Budapest, 2000), Vol. 24B, European Physical Society, Geneva (2001) CD-ROM file P1.041.
[10] Yoshino, R., et al., in Fusion Energy 1998 (Proc. 17th Int. Conf. Yokohama, 1998), IAEA, Vienna (2000) CD-ROM file ITERP1/14 and http://www.iaea.org/programmes/ripc/physics/fec2000/html/node1.htm.

[11] Sykes, A., Phys. Plasmas **4** (1998) 1665.
[12] Morel, K.M., et al., J. Nucl. Mater. **266–269** (1999) 1040.
[13] Counsell, G.F., Ahn, J.W., Fielding, S.J., Maddison, G.P., in Controlled Fusion and Plasma Physics (Proc. 27th Eur. Conf. Budapest, 2000), Vol. 24B, European Physical Society, Geneva (2001) CD-ROM file P4.088.

(Manuscript received 8 October 2000
Final manuscript accepted 25 April 2001)

E-mail address of A. Sykes:
alan.sykes@ukaea.org.uk

Subject classification: B0, Te; C0, Te; F1, Te; G6, Te; I2, Te; J1, Te